AGU PUBLICATIONS

JGR

Journal of Geophysical Research: Atmospheres

RESEARCH ARTICLE

10.1002/2013JD021150

Key Points:
- Partition of surface radiative fluxes into turbulent and conductive heat fluxes
- Maximum entropy production theory-based method
- Temperature/humidity gradient and wind speed independent algorithm of fluxes

Correspondence to:
J. Wang,
jingfeng.wang@ce.gatech.edu

Citation:
Wang, J., R. L. Bras, V. Nieves, and Y. Deng (2014), A model of energy budgets over water, snow and ice surfaces, *J. Geophys. Res. Atmos.*, *119*, 6034–6051, doi:10.1002/2013JD021150.

Received 7 NOV 2013
Accepted 9 MAY 2014
Accepted article online 13 MAY 2014
Published online 30 MAY 2014

A model of energy budgets over water, snow, and ice surfaces

Jingfeng Wang[1], Rafael L. Bras[1], Veronica Nieves[2], and Yi Deng[1]

[1]Georgia Institute of Technology, Atlanta, Georgia, USA, [2]Jet Propulsion Laboratory, California Institute of Technology, Pasadena, California, USA

Abstract The recently formulated maximum entropy production (MEP) model over land surfaces has been generalized to water-snow-ice surfaces. Analytical solutions of energy budget in terms of the partition of surface radiative fluxes into (turbulent and/or conductive) heat fluxes at the earth-atmosphere interface are derived as functions of surface temperature (e.g., sea surface temperature). The MEP model does not require data of wind speed, air temperature-humidity, and surface roughness. Test of the MEP model using observations from several field experiments is encouraging. Potential applications of the proposed model for understanding long-term trends in surface heat fluxes and for closing global surface energy budget at the Earth's atmosphere are suggested.

1. Introduction

Weather and climate are driven by the solar energy that enters the Earth system through its partition into water vapor (latent heat) and thermal energy (sensible heat) fluxes over the Earth's surface. Parameterization of the energy budget over the Earth's surface has been the central component of land (ocean) surface schemes in the coupled land-ocean-atmospheric models. Over the past 50 years, a number of land surface models (LSMs) of various levels of complexity have been developed for parameterizing heat fluxes, among other land surface processes, for numerical simulations of regional and global weather and climatic processes. Commonly used LSMs include the Biosphere-Atmosphere Transfer Scheme (BATS) [*Dickinson et al.*, 1986; *Yang and Dickinson*, 1996], the Community Atmosphere-Biosphere-Land Exchange (CABLE) model [*Kowalczyk et al.*, 2006; *Wang and Bras*, 2011], the Community Land Model (CLM) [*Dai et al.*, 2003; *Oleson et al.*, 2010], the Joint UK Land Environment Simulator (JULES) model [*Blyth et al.*, 2010; *Best et al.*, 2011], the joint National Centers for Environmental Prediction LSM, Oregon State University LSM, Air Force Weather Agency and Air Force Research Lab LSM, and the National Weather Services Hydrologic Research Lab LSM (NOAH) model [*Mitchell*, 2005; *Lemone et al.*, 2008]. All LSMs use bulk transfer formulas (flux-gradient methods), i.e., the linear equations relating fluxes to the corresponding scalar-gradients multiplied by empirical or semiempirical wind speed-dependent transfer coefficients, to parameterize the surface latent and sensible heat fluxes. A comprehensive and critical evaluation of some 20 LSMs in early 1990s [*Henderson-Sellers et al.*, 1995] concluded that no single (existing) land surface model is capable of capturing all features of the surface energy balance under all conditions [*Desborough et al.*, 1996; *Henderson-Sellers et al.*, 2003]. The situation has not changed 20 years later [*Mueller et al.*, 2011]. Even with the new generation of LSMs such as BATS, CABLE, CLM, JULES, and NOAH resulting from years of efforts to improve the representations of land surface processes, we still face the challenges of modeling energy budget over the Earth (land, ocean, snow ice) surfaces.

Parameterization of latent heat flux or evaporation has always been a major challenge in the LSMs using the bulk transfer method. For example, latent heat flux tends to be underestimated and sensible heat flux overestimated in the NOAH model [*Lemone et al.*, 2008], while it is often overestimated in the JULES model [*Blyth et al.*, 2010]. The difficulties of the LSMs in parameterizing the surface fluxes are caused by several limitations of the bulk transfer method. First, bulk transfer modeled heat fluxes are not constrained by conservation of energy. Second, the bulk gradient variables (differences between two comparable numbers) are subject to large measurement errors. Third, uncertainties in the wind spend and/or surface roughness-dependent transfer coefficients amplify the measurement errors of model input. The bulk transfer model is the only method for modeling the surface fluxes over oceans [*Saunders*, 1967; *Liu et al.*, 1979; *Fairall et al.*, 1996a; *Curry et al.*, 1999; *Chou et al.*, 2003; *Large and Yeager*, 2009]. It has been well recognized [*Kiehl and Trenberth*, 1997] that the bulk transfer-based fluxes estimates are strongly affected by the measurement error of wind speed data. In addition, the measurement errors of temperature and moisture gradients also cause

modeling error of the bulk transfer-based fluxes. The measurement and modeling errors of the input variables of the bulk transfer formula lead to substantial uncertainties of the modeled fluxes, especially at subdaily and regional/global scales using remote sensing observations [*Zeng et al.*, 1998]. Without constrains on radiation energy, the bulk transfer-based surface fluxes tend to be underestimated under weak wind condition and overestimate under strong wind conditions. Violation of conservation of energy is arguably the primary cause of the inconsistent seasonality of the existing global ocean surface fluxes data as wind speed negatively correlates with solar radiation at seasonal scales [*Moore and Renfrew*, 2002]. Further improvement of parameterization of energy budget in LSMs takes a radically different approach to overcome these difficulties.

The recently proposed method based on the theory of maximum entropy production (MEP) provides a new approach for modeling the surface energy budget. Contrary to the classical bulk transfer models, the MEP method allows the parameterization of the fluxes satisfying the conservation of energy without using gradient variables, wind speed, surface roughness, and other empirical parameters in the transfer coefficients. The MEP model of energy budget over the land surfaces [*Wang and Bras*, 2009, 2011] is the first moisture-gradient independent evaporation model. The goal of this study is to generalize the MEP model, originally formulated for land (bare sols and canopy) surfaces, to parameterize evaporation and heat fluxes over water-snow-ice surfaces. The MEP method is a statistical approach built upon the Bayesian probability theory for making prediction given incomplete information about any systems [*Jaynes and Bretthorst*, 2003]. The MEP theory may be understood as an application of the principle of maximum entropy (MaxEnt) first proposed as a method of assigning probability distributions in statistical mechanics [*Jaynes*, 1957] and now known and used as a general inference algorithm. The MaxEnt method has many successful applications in science and engineering [e.g., *Kapur*, 1989] including meteorology [*Suzuki*, 1958; *Hayashi*, 1981; *Verkley and Lynch*, 2009]. The relatively new MEP method [*Dewar*, 2005, 2013], motivated by an intuitive concept [*Paltridge*, 1975] introduced in a climatic study, has been applied to a growing number of subjects [*Kleidon and Lorenz*, 2005] including land surface hydrology [*Kleidon and Schymanski*, 2008] and bioecological systems [*Kleidon et al.*, 2010; *Shipley*, 2010]. The formulation of the MEP model of energy budget is described in *Wang and Bras* [2009, 2011]. A key step is to formulate a "dissipation function" (or "entropy production function") to characterize the fundamental physics underlying evaporation and transport processes. In this paper we report the formulation and test of the MEP model using in situ observations from field experiments over a lake, the Pacific Ocean off California coast, snow-covered grassland, and Arctic sea ice sheet.

2. Model Formulation

2.1. Energy Balance Equation Over Water-Snow-Ice Surfaces

In this study, the Earth's surface is treated as a mathematical surface without volume. Energy balance over the Earth's surface is a representation of the conservation of energy, i.e., radiation, turbulent, and conductive energy fluxes sum to zero. A general expression of the conservation of energy over the Earth's surface is written as

$$R_n + R_0 - E - H - Q = 0, \tag{1}$$

where R_n is the net radiation defined as

$$R_n \equiv \left(R_s^d + R_s^u\right) + \left(R_l^d + R_l^u\right) \equiv R_s^n + R_l^n, \tag{2}$$

where R_s^d is the incoming solar radiative flux, R_s^u the reflected solar flux, R_0 the solar radiation entering the solid or liquid media, R_l^u the emitted long-wave radiative flux from the surface, R_l^d the downward atmospheric long-wave radiative flux, E the latent heat flux (evaporation), H the sensible heat flux into the atmosphere, and Q is the surface thermal energy flux of the solid/liquid media. Radiative fluxes toward (away from) the surface are defined as positive (negative), while turbulent and conductive heat fluxes away from (toward) the surfaces are defined as positive (negative).

Depending on the transparency of the surface to sunlight, a separate energy balance equation of solar radiation may be needed to relate R_n to R_0 in equation (1). Since absorption of solar radiation by soils occurs within a layer of infinitesimal depth on the order of micrometers, soil is considered nontransparent to sunlight for the purpose of modeling energy budget. Therefore, R_0 vanishes over the land surfaces and equation (1) becomes

$$R_n = E + H + Q, \tag{3}$$

where Q is known as the ground heat flux (often denoted by G in hydrology literature). Since absorption of solar radiation by water-snow-ice occurs within a layer of finite depth on the order of meters, water-snow-ice media are considered transparent to sunlight, leading to a separate solar radiation energy balance equation; i.e., $R_s^n + R_0 = 0$. Then the energy balance equation over water-snow-ice surfaces, equation (3), reduced to [*Fairall et al.*, 1996b]

$$R_l^n = E + H + Q. \tag{4}$$

Equations (3) and (4), the energy balance equations over lands (soil/vegetation) and water-snow-ice surfaces respectively, are identical only for nighttimes. Note that the sign of Q here is opposite to that commonly defined in oceanography.

2.2. MEP Model Formulation

The MEP model of heat fluxes can be derived by minimizing the "dissipation function" or "entropy production function" expressed in terms of the heat fluxes under the constraint of the surface energy balance equation (4). The mathematical definition of the dissipation function in terms of Shannon information entropy was described in *Wang and Bras* [2009, 2011]. The concept of dissipation function may be intuitively understood using an analogy of thermal dissipation produced by electric current passing through resistors [*Wang et al.*, 2013]. The analogy highlights the mathematical structure and physical significance of the MEP theory. For the case of fluxes at the earth-atmosphere interface, the generalized dissipation function in the MEP formulation may be obtained by replacing the electric currents with the heat fluxes and the (reciprocal) impedances with the thermal inertia parameters associated with the individual heat fluxes [*Wang and Bras*, 2009, 2011]. It is important to emphasize that the dissipation (entropy production) function defined in *Wang and Bras* [2009, 2011] is not limited to the cases of thermal energy dissipation. The dissipation function defined for the heat fluxes over the Earth's surface [see *Wang and Bras*, 2011, equation (1)] is not related to the thermal energy dissipation function. It is a general expression of information entropy in terms of observables (fluxes) derived from the application of the maximum entropy principle in the context of the Bayesian probability theory.

Since heat transfer near a material surface is due to either molecular or turbulent diffusion, the corresponding thermal inertia parameters need to be parameterized accordingly. Previous observational studies [e.g., *Khundzhua et al.*, 1977] have confirmed that under common meteorological conditions (e.g., wind speed < 15 m s^{-1} [e.g., *Boyle*, 2007]), a thin water layer referred to as cool skin exists next to the water-atmosphere interface where heat transfer is through thermal conduction [*Fairall et al.*, 1996b]. In this study, the MEP model is formulated for the case of cool skin so that the corresponding thermal inertia parameter only depends on the physical property of (still) liquid water. It is conceptually straightforward to express the thermal inertia in terms of eddy diffusivity parameterized based upon boundary layer turbulence models.

As a result of this analogy [see *Wang and Bras*, 2011, equation (1)], the dissipation function D involving the surface fluxes E , H, and Q is postulated as

$$D(E,H,Q) = \frac{2E^2}{I_e} + \frac{2H^2}{I_a} + \frac{2\left(R_s^n + Q\right)^2}{I_{\mathrm{wsi}}}, \tag{5}$$

where I_e and I_a and I_{wsi} are the thermal inertia parameters associated with the corresponding heat fluxes. I_{wsi} ($= \sqrt{\rho c \lambda}$ with the density ρ, the specific heat c, and the thermal conductivity λ of water-snow-ice media) is a physical property of water-snow-ice (1.56×10^3 J m^{-2} K^{-1} s$^{-1/2}$ for still liquid water, 1.92×10^3 J m^{-2} K^{-1} s$^{-1/2}$ for ice, and ~ 0.6–1.4×10^3 J m^{-2} K^{-1} s$^{-1/2}$ for snow with density varying between 100 and 500 kg m^{-3} [e.g., *Yen*, 1981]). I_a and I_e have been formulated [*Wang and Bras*, 2009, 2011] based on an extremum solution of Monin-Obukhov similarity equations [*Wang and Bras*, 2010]:

$$I_a = \rho c_p \sqrt{C_1 \kappa z}\left(C_2 \frac{\kappa z g}{\rho c_p T_r}\right)^{\frac{1}{6}} \mid H \mid^{\frac{1}{6}} \equiv I_0 \mid H \mid^{\frac{1}{6}}, \tag{6}$$

$$I_e = \sigma I_a, \tag{7}$$

where ρ is the density of the air, c_p the specific heat of the air at constant pressure, κ the von Kármán constant ($\sim$0.4), z a local topography-dependent reference height above the surface (see *Wang and Bras*

[2009, Table 2], for more details), g the gravitational acceleration, T_r a reference temperature (~ 300°K), C_1 and C_2 two universal empirical constants characterizing the effect of stability on the profiles of potential temperature and wind velocity [see *Wang and Bras*, 2009, p. 4]. Assuming that water vapor right above water-snow-ice surface is in equilibrium with the liquid/solid water, the dimensionless parameter σ in equation (7) is given by

$$\sigma = \sqrt{\alpha}\frac{\Delta}{\gamma}, \tag{8}$$

where Δ is the slope of the saturation water vapor pressure curve at the surface temperature T_s according to Clausius-Clapeyron equation, γ the psychrometric constant, and α is the ratio of eddy diffusivity of turbulent transport of water vapor to that of heat. In general, σ is a function of T_s and surface specific humidity [see *Wang and Bras*, 2011, equation (4)]. Earlier studies [e.g., *Andreas and Murphy*, 1986] suggested that α for the case of water surface is unity and is often assumed to be unity over solid surfaces.

The postulation of D as in equation (5) is made using an analogy to the case of land surfaces [see *Wang and Bras*, 2011, equation (1)]. Transparency of water-snow-ice media to sunlight suggests R_s^n be included in D as $R_s^n + Q$ is the total energy flux at the surface of a water-snow-ice layer, just like ground heat flux being the energy flux at the surface of a soil layer not transparent to sunlight. This postulation will be justified through its predictive capability shown in section 4.

2.3. MEP Model of *E*, *H*, and *Q*

According to the MEP formalism, extremizing D in equation (5) under the constraint of the surface energy balance as in equation (4) for given R_s^n, R_l^n, and T_s leads to the simultaneous solution of E, H, and Q :

$$\left[1 + B(\sigma) + \frac{B(\sigma)}{\sigma}\frac{I_{\mathrm{wsi}}}{I_0} \mid H \mid^{-\frac{1}{6}}\right] H = R_n, \tag{9}$$

$$E = B(\sigma)H, \tag{10}$$

$$Q = R_l^n - E - H, \tag{11}$$

where

$$B(\sigma) = 6\left(\sqrt{1 + \frac{11}{36}\sigma} - 1\right). \tag{12}$$

Equation (9) is a nonlinear algebraic equation of H that can be solved numerically. Once H is obtained from equation (9) for given R_n and T_s, the solution of E and Q follow from equations (10) and (11), respectively. B in equation (10) is recognized as the reciprocal Bowen ratio expressed in terms of surface temperature-dependent σ given in equation (8). Equations (9)–(11) are referred to as the MEP model of heat fluxes at water-snow-ice surfaces, which is formally identical to that over the (saturated) land surfaces. Note that the MEP solution of E and H only uses data of T_s and R_n, while that of Q needs additional data of R_s^n or R_l^n. This feature of the MEP model reflects the fact that solar radiation is the primary energy source of the heat flux within a water-snow-ice layer. In contrast, the MEP solution of Q over the land surfaces (i.e., ground heat flux) is not directly affected by the partition of R_n into R_s^n and R_l^n since the solar radiation does not penetrate soils. The confirmation of the MEP solution of Q according to shown below indirectly justifies the postulated dissipation function as in equation (5) .

Summary of the MEP Model Formulation: Table 1 lists the model input and parameters. Model input variables used in equations (9)–(11) are R_n, R_l^n, and T_s. Model parameters are those included in the expressions of I_0 and σ given in equations (6) and (8), respectively. All model parameters are physical variables. The MEP model formulation does not use empirical tuning parameters.

Table 1. The Inputs and Parameters of the MEP Model of Surface Fluxes E, H, and Q According to Equations (9)–(11)[a]

Modeled Fluxes	Model Inputs	Model Parameters	Constant Parameters
E, H	R_n, T_s	z	$c_p, g, C_1, C_2, I_{wsi}, T_r$
Q	R_n, R_l^n, T_s	α	γ, κ, ρ

[a] z, the distance above the surface, is taken as $z = 0.2$–0.3 m for water surfaces (with conductive "cool skin") and $z = 2$–3 m for snow ice surfaces. α, the ratio of eddy diffusivity of turbulent transport of water vapor versus that of heat, is commonly assumed to be unity. $c_p = 1004$ J kg^{-1} K^{-1} is the specific heat of the air at constant pressure, $g = 9.8$ m s^{-2} the gravitational acceleration, the universal constants in the Monin-Obukhov similarity equations $C_1 \simeq 2$ (unstable) or 0.7 (stable), $C_2 \simeq 5$ (unstable) or 10 (stable), I_{wsi} the thermal inertia of water-snow-ice media, $T_r \sim 300$ K the representative (reference) temperature of the environment, γ the psychrometric constant, $\kappa \simeq 0.4$ the von Kármán constant, and ρ the density of air. γ and ρ vary linearly with the atmospheric pressure P following $\gamma = c_p L_v^{-1} m_d m_v^{-1} P$ (the latent heat of vaporization of liquid water $L_v = 2.5 \times 10^6$ J kg^{-1}, the molecular weight of water vapor $m_v = 18$ g mol^{-1} and that of dry air $m_d = 29$ g mol^{-1}) and the ideal gas law, respectively.

2.4. On the MEP Model

The MEP theory, a statistical method or an inference algorithm, was used for finding the most probable solutions when the available information is not sufficient to obtain definite answers. The model formulation described above was to seek an answer to the question: what would be the most probable energy budget given the radiation fluxes and surface temperature? The derivation of the fluxes from only the information of radiation and temperature should not be interpreted as that the transport of water vapor and heat are physically only dependent on radiation and surface temperature. The effects of other environmental conditions such as wind (or wind shear), temperature/moisture gradient, and atmospheric pressures have been taken into account through the thermal inertia parameters (i.e., I_e and I_a in equations (6) and (7)). For example, the effect of wind speed on the turbulent transport in the boundary layer is represented through the formulation of I_a even though wind speed is not explicitly included in the expression of I_a as wind speed (shear) is expressed as a function of sensible heat flux according to the extremum solution of the Monin-Obukhov similarity equations. In fact, all the environmental variables used in the classical models are included explicitly or implicitly in the model formulation. The MEP formulation of fluxes in terms of radiation and surface temperature implies that the MEP theory allows the most effective use of the data with the redundancy of the physically coupled environmental variables about the fluxes removed by the MEP formalism. Parsimony of the MEP model in input variables and model parameters substantially reduces the uncertainties of the MEP-modeled fluxes. In particular, without explicitly using wind speed, temperature/moisture gradient, and surface roughness as model inputs and parameters further reduces the modeling errors of the fluxes. Uncertainties of the MEP-modeled fluxes are limited by the measurement errors of radiation fluxes, which are on the order of 10% or less. Uncertainties in the MEP-modeled fluxes caused by other input and model parameters are more limited. For example, the measurement error of skin temperature (δT_s) is quite small, on the order of $\delta T_s / T_s \sim 3/300 = 1\%$.

3. A Physically Based Model of Q

For the thermal conduction within the water cool skin and snow/ice layer, there exists an analytical expression of Q in terms of T_s and R_s^n, referred to as the physically based model of Q herein, similar to the relationship between ground heat flux and surface soil temperature known as half-order time derivative/integral [*Wang and Bras*, 1999]. Since the temperature-gradient independent expression of Q according to equations (9)–(11) is obtained without solving physical principles-based equations, the MEP formulation of Q is justified if the two models agree.

Assuming horizontal homogeneity, the heat conduction within sunlight transparent media may be described by a one-dimensional inhomogeneous diffusion equation with a heating source resulting from the absorption of solar radiation [*Kaiser and Williams*, 1974; *Soloviev and Schlüssel*, 1996]:

$$\frac{\partial T}{\partial t} = \kappa \frac{\partial^2 T}{\partial z^2} + \frac{\partial}{\partial z}\left[\frac{R_s^n(t)}{\rho c} I(z)\right] \tag{13}$$

$$T = T_0, \quad \text{for} \quad t = 0, \quad z < 0, \tag{14}$$

$$T = T_0, \quad \text{for} \quad t > 0, \quad z \to -\infty \tag{15}$$

where $T(z, t)$ is the water-snow-ice temperature, T_0 a constant deep water temperature, $I(z)$ the (dimensionless) solar radiation absorption profile of water-snow-ice, and ρ, c, κ the density, specific heat, and thermal diffusivity of (still liquid) water-snow-ice, respectively. The vertical coordinate z points upward with $z = 0$ at the material surface. No boundary condition is prescribed at the surface, which allows the most generic relationship linking Q to T_s and R_s^n. It is important to emphasize that the mathematical infinity in equation (15), which makes analytical solution possible, should be interpreted as that the conductive cool skin is very shallow relative to the depth of the mixed-layer for the case of water. In fact, only the solution of equations (13)–(15) at the surface ($z \to 0$) is of interest for the purpose of relating Q analytically to T_s and R_s^n as in the MEP model of Q according to equations (9)–(11).

A generic expression of $I(z)$ is the generalized Beer's law:

$$I(z) = \sum_{i=1}^{N} F_i \exp\left(\frac{z}{\zeta_i}\right), \tag{16}$$

where N is the number of wavelength bands, F_i the extinction coefficient, and ζ_i the characteristic penetration depth corresponding to the ith wavelength band. For seawater, nine extinction coefficients have been ($N = 9$ in equation (16)) identified according to experimental studies [*Defant*, 1961]. The coefficients F_i and ζ_i reported by *Defant* [1961] and used previously [*Paulson and Simpson*, 1981] will be used in this study. For snow/ice, I follows a simple Beer's law ($N = 1$ in equation (16)) [*Colbeck*, 1989; *Greuell and Oerlemans*, 1989] with a bulk extinction coefficient dependent on the bulk density of snow/ice.

Equations (13)–(16) lead to an analytical expression of Q in terms of T_s and R_s^n (a derivation is given in Appendix A):

$$\begin{aligned} Q(t) = {} & \frac{I_{\text{wsi}}}{\sqrt{\pi}} \int_0^t \frac{\partial T_s(\tau)}{\partial \tau} \frac{\mathrm{d}\tau}{\sqrt{t-\tau}} - \left(\sum_{i=1}^{N} \frac{\sqrt{\kappa}}{\zeta_i} F_i\right) \frac{1}{\sqrt{\pi}} \int_0^t \frac{R_s^n(\tau)\mathrm{d}\tau}{\sqrt{t-\tau}} \\ & + \int_0^t \sum_{i=1}^{N} \left[\left(\frac{\kappa}{\zeta_i^2} F_i\right) \mathrm{e}^{\frac{\kappa}{\zeta_i^2}(t-\tau)} \operatorname{erfc}\left(\frac{\sqrt{\kappa}}{\zeta_i}\sqrt{t-\tau}\right)\right] R_s^n(\tau)\mathrm{d}\tau \end{aligned} \tag{17}$$

where erfc is the complementary error function and τ the integration (time) variable. A numerical algorithm for calculating the integrals in equation (17) is given in Appendix B. The integration starts from an arbitrary time when the temperature profile is close to uniform or Q close to zero within the conductive layer. Case studies [e.g., *Wang and Bras*, 1999] suggest that Q is not sensitive to the hypothetical initial uniform temperature profile when t is on the order of a few hours.

The analytical solution of Q, referred as a physically based model of Q, is completely independent of the MEP model of Q formulated in section 2 since the governing equation (13) is independent of the turbulent model used in parameterizing I_a and I_e of the MEP model. Yet the physically based model and the MEP model predicted Q are consistent as demonstrated in section 4.2.3 below.

Equation (17) can be written in an equivalent form where T_s is expressed in terms of Q and R_s^n (according to equation (A9)):

$$T_s(t) = T_0 + \frac{1}{\rho c} \int_0^t \sum_{i=1}^{N} \left[\frac{F_i}{\zeta_i} \mathrm{e}^{\frac{\kappa}{\zeta_i^2}(t-\tau)} \operatorname{erfc}\left(\frac{\sqrt{\kappa}}{\zeta_i}\sqrt{t-\tau}\right)\right] R_s^n(\tau)\mathrm{d}\tau + \frac{1}{I_{\text{wsi}}} \int_0^t \frac{Q(\tau)\mathrm{d}\tau}{\sqrt{\pi(t-\tau)}}. \tag{18}$$

4. Model Test

The MEP model of E, H, and Q will be tested against field observations of heat fluxes. Direct measurements of Q are much more difficult than those of E and H over the water-snow-ice surfaces. We are aware of only one experimental technology for directly measuring Q over water surfaces [*Sromovsky et al.*, 1999a, 1999b; *Boyle*, 2007], which, to our knowledge, has not been deployed in field experiments. Snow heat flux can be

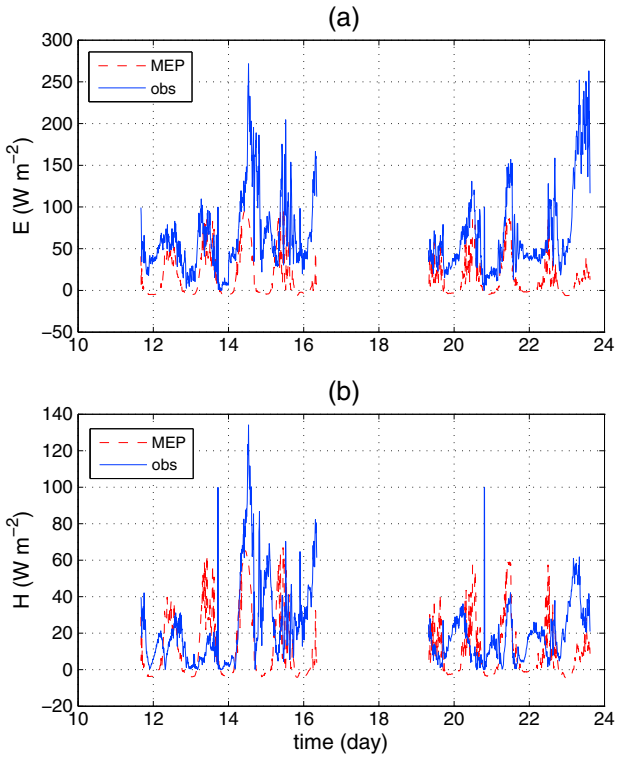

Figure 1. MEP model-predicted (broken red) (a) latent heat flux E and (b) sensible heat flux H, according to equations (9) and (10) using measured R_n and T_s, versus observational fluxes (solid blue) for Lake Råksjö from NOPEX experiment during 10–24 June 1994.

measured using soil heat flux sensors as those deployed during the Surface Heat Budget of the Arctic Ocean (SHEBA) experiment. However, measuring snow heat flux at surface Q is difficult due to changing snow depth and disturbances from solar radiation. We are unaware of publicly available field data products of Q at the snow/ice surfaces. Therefore, the "observed" Q in this study is obtained as the residual of the energy balance equation (4) where the three terms on the left-hand side are from field observations. Only publicly available data sets are used in this study.

4.1. Test of the MEP Model of *E* and *H*

4.1.1. Water Surface

Two field experiment data sets were used in this study. The Northern Hemisphere Climate Processes Field Experiment (NOPEX) provides an open access data set of eddy covariance measurements of turbulent fluxes over two lakes, Råksjö (1.5 km^2 in surface area and 4 m in depth) and Tämnaren (37 km^2 and 2 m), over short periods of time during June and July of 1994 [*Halldin et al.*, 1999]. These eddy covariance data were used to calibrate the transfer coefficients of a bulk transfer model used for estimating the turbulent heat fluxes. More details about the field experiment and the data set are described in *Heikinheimo et al.* [1999]. Due to technical difficulties of collecting data from eddy covariance device on a floating platform over the lakes, the eddy covariance measurement of turbulent fluxes are subject to substantial uncertainty. For example, the wind-caused measurement errors were on the order of 10 W m^{-2} for sensible heat flux and 100 W m^{-2} for latent heat flux when wind speed is 5–6 m s^{-1} or higher.

California Research at the Nexus of Air Quality and Climate Change 2010 (CALNEX2010) field experiment [*Ryerson et al.*, 2013] collected eddy covariance turbulent fluxes and other meteorological data from the NOAA R/V *Atlantis* Ship cruise along the California coast during 14 May to 7 June 2010 [*Wolfe and Fairall*, 2010]. The ship carried eddy covariance system and other devices placed at 15–19 m above sea surface-measured turbulent fluxes, atmospheric and oceanic variables. The sea surface (skin) temperature was not available. Water temperature at 5 cm depth was used in this study. More information about CALNEX2010 cruise track and data products can be found at www.esrl.noaa.gov/csd/projects/calnex/.

Figure 1 compares the MEP model predicted E and H (in broken red), according to equations (9) and (10) using the observed R_n and T_s, with the fluxes data (in solid blue) for Lake Råksjö. Conductive layer of cool skin is expected to prevail during this period of time as wind speed (Figure 2a) was significantly weaker than 15 m s^{-1} threshold [e.g., *Boyle*, 2007]. Figure 1 shows that the MEP-modeled fluxes agree with the data qualitatively. The diurnal cycle of MEP-modeled E and H are consistent with the observed E and H, and their magnitudes are comparable while the agreement is closer under the condition of lower wind speed (e.g., $U < 6$ m s^{-1}). The nighttime modeled fluxes tend to be lower than the data. Note that the bulk transfer method tends to overestimate nighttime fluxes as the transfer coefficients were taken as constant [*Heikinheimo et al.*, 1999]. A more realistic parameterization of transfer coefficients should take the diurnal variation of the stability of the surface layer into account; i.e., the constant transfer coefficients for nighttime as those for daytime would overestimate the nighttime turbulent fluxes. The error associated with the constant transfer coefficients is compounded with more severe limitation of the bulk transfer method:

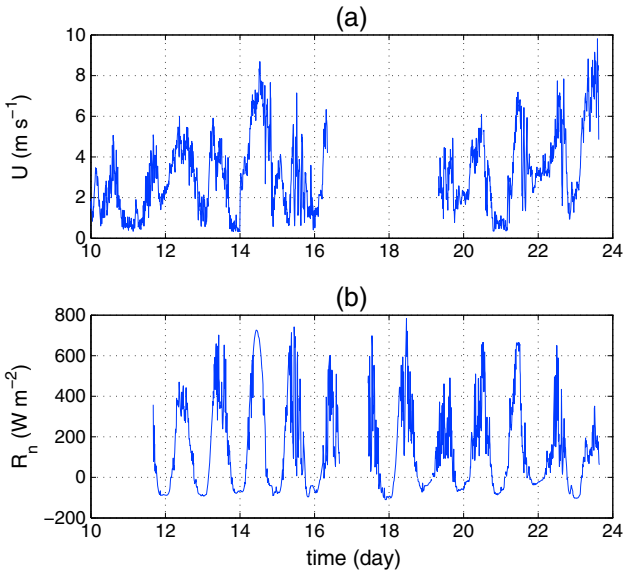

Figure 2. (a) Net radiation R_n and (b) wind speed U measurements over Lake Råksjö from the NOPEX experiment during 10–24 June 1994.

lack of constrain of energy balance leading to substantial uncertainty in the fluxes data. Nonetheless, the comparable magnitudes of the modeled versus observed fluxes suggests that the MEP model is able to capture the turbulent fluxes as a partition of radiation at water surface given only the surface temperature. Not affected by the uncertainty of the near-surface wind speed, air temperature, humidity, and surface roughness, the uncertainty of the MEP-modeled fluxes is limited when the radiation data are adequately accurate. Specifically, the largest differences between the MEP-modeled and observed E and H occurred on 23 June when wind was stronger up to 8–9 m s^{-1} over the 2 week period (excluding the missing data days). The MEP-modeled E and H on 23 June were the lowest during this period, which is consistent with the lowest R_n. Specifically, as the peak R_n drops from ~400 W m^{-2} on day 22 to 200 W m^{-2} on day 23 (Figure 2b), the MEP model predicted E reduces by half, while the bulk transfer method predicted E nearly doubles (from 100 W m^{-2} to 200 W m^{-2}; see Figure 1a). According to *Heikinheimo et al.* [1999], E was expressed in terms of surface specific humidity gradient multiplied by wind speed and constant transfer coefficient. The drastic increase in the bulk transfer-based E is apparently caused largely by stronger wind (from 6 m s^{-1} to 8 m s^{-1}; see Figure 2a). This increasing trend of E contradicts the decreasing trend of R_n as the energy source of evaporation. Therefore, the MEP model predicted E is arguably more reliable than the bulk transfer-based data that are subject to violation of energy conservation. More comprehensive and quantitative analysis of the MEP-modeled fluxes needs higher-quality in situ fluxes data products.

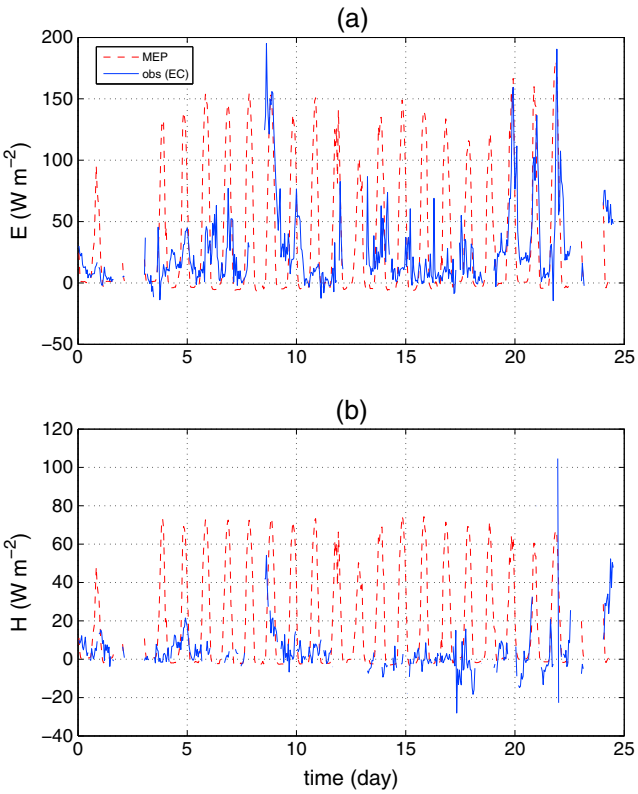

Figure 3. MEP model-predicted (broken red) (a) latent heat flux E and (b) sensible heat flux H, according to equations (9) and (10) using measured hourly net radiation R_n and sea snake temperature at 0.05 m depth T_s, versus eddy covariance fluxes (solid blue) from the CALNEX cruise during 14 May to 7 June 2010.

Figure 3 compares the MEP model-predicted E and H (in broken red), according to equations (9) and (10) using the observed R_n and T_s (5 cm depth water temperature), with the eddy covariance fluxes data (in solid blue) from the CALNEX2010 cruise. Like the case of Lake Råksjö, conductive layer of cool skin is expected to prevail during the cruise as wind speed was mostly below 10 m s^{-1} (Figure 4a). The

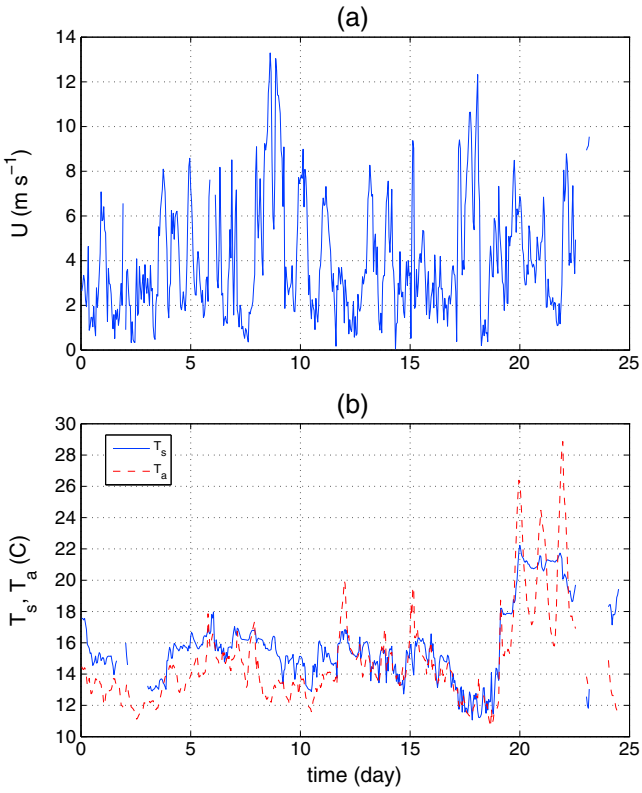

Figure 4. (a) Wind speed U and (b) water temperature T_s at 0.05 m depth and air temperature T_a at 15–19 m above the sea surface from the CALNEX cruise during 14 May to 7 June 2010.

MEP model-predicted E is in reasonable agreement with the observed E for 23 May (day 9) and 3–7 June (days 20–24). The MEP-predicted H is consistent with the observed H for these days except that there are more missing data. During the other days of this period, MEP-predicted E and H were much higher than the eddy covariance fluxes. The closer agreement between the modeled and observed fluxes concurred with either stronger wind or greater sea surface and air temperature gradient (see Figure 4). It appears that the eddy covariance devices on the ship about 19 m above the sea surface did not capture the turbulent fluxes when wind speed and sea-air temperature gradient are relatively weak. In fact, the meteorological environment during the CALNEX2010 cruise was rather similar to the lake Råksjö during 10–24 June 1994 (see Figure 2 for wind speed and net radiation data). The net radiation during the CALNEX2010 cruise was at the level of 900 W m^{-2} (diurnal peak, data not shown), while that over lake Råksjö was the level of 700 W m^{-2} (diurnal peak shown in Figure 2b). Wind speed was comparable (Figure 4a for CALNEX2010 and Figure 2a for lake Råksjö), and water surface temperature almost identical around 15°C (Figure 4b for CALNEX2010 and not shown for lake Råksjö). Therefore, the turbulent fluxes are expected to be comparable from the two field experiments. E on the order of ~100–150 W m^{-2} and H on the order of ~60 W m^{-2} were recorded by the eddy covariance device placed 2–3 m above the lake surface. But $E < 50$ W m^{-2} and $H < 10$ W m^{-2} were obtained from the eddy covariance device placed 15–19 m above the sea surface except for 23 May and 3–7 June when stronger wind and greater air-sea temperature gradient occurred. The low eddy covariance turbulent fluxes are inconsistent with the condition of net radiation, water surface temperature, and wind speed. This is the evidence that the ship observations tend to underestimate the air-sea turbulent fluxes under condition of weak wind and air-sea temperature gradient due to the extra height of eddy covariance device on large ships like R/V *Atlantis*. The MEP model is able to predict the turbulent fluxes consistent with the radiant energy and meteorological conditions even though wind speed and air-sea temperature gradient are not explicitly used in the model formulation. See below for more discussions on the effect of near-surface meteorological condition on the turbulent fluxes.

Evaporation from water surfaces is traditionally estimated using two approaches: the bulk transfer equations relating water vapor flux to water vapor gradient with a wind speed-dependent transfer coefficient and the Penman equation that partitions radiant energy into evaporation and sensible heat flux. Wind speed versus radiant energy as the main driver of free water evaporation is under debate. *Granger and Hedstrom* [2011] concluded that "for time periods shorter than daily, the open water evaporation bears no relationship to the net radiation," while the measured evaporation using scintillometer reported in *McJannet et al.* [2011] shows that evaporation is closely correlated with net radiation. It has been known [*Slatyer and McIlroy*, 1961, pp. 3–14] that the measurement of evaporation (by atmometer) "overestimates the effect of wind and underestimates that of (net) radiation." This tendency compounded with the highly variable near-surface temperature and humidity gradient may be responsible, at least partly, for the discrepancies between the MEP model-predicted E and H and the fluxes derived from the bulk transfer equations where

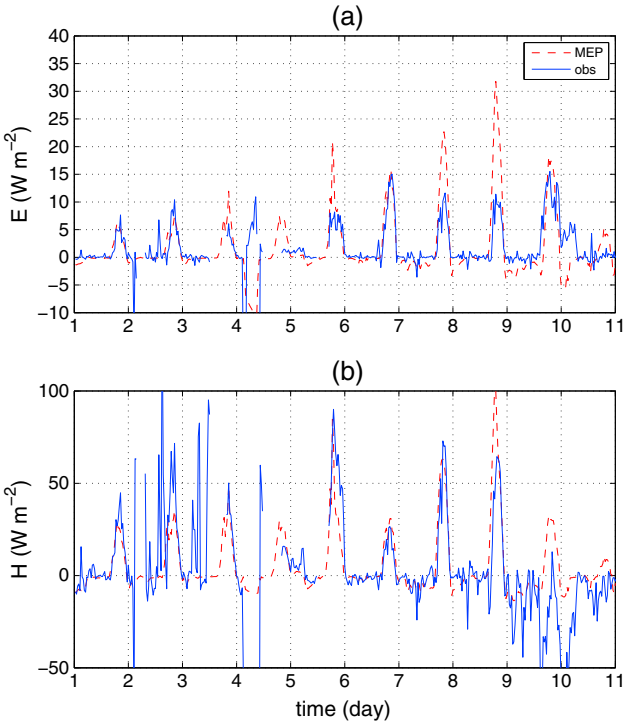

Figure 5. MEP model-predicted (broken red) (a) latent heat flux E and (b) sensible heat flux H, according to equations (9) and (10) using measured R_n and T_s, versus measured fluxes (solid blue) at FLUXNET site, grassland in Lethbridge, Alberta, Canada, during 1–10 December 2007.

wind speed and the associated measurement errors tend to cause large and unknown error in the estimated evaporation over water surfaces.

This case study highlights the challenges in producing accurate data of turbulent fluxes over water surfaces due to technical and computational difficulties. Over lakes and oceans movable floats carrying devices cause significant uncertainty in wind velocity data that affects both eddy covariance-based and bulk-transfer-based estimates of turbulent heat fluxes. Turbulent fluxes data derived using bulk transfer equations are also subject to uncertainty in the measurements of temperature and moisture gradient. It has been known that rapid changes of temperature and humidity near the surface within a shallow layer up to 25 cm [see *Caisley et al.*, 1963, Figure 11] cause the bulk gradients of temperature and humidity near the surface to be drastically different from the local gradients associated the surface fluxes. Analysis of eddy covariance fluxes data over a lake surface [*Yang et al.*, 2013] showed that the relative efficiency of evaporation (ratio of E to H) over lake surface tends to decreases with height. This is consistent with the NOPEX and CALNEX2010 data (Figures 1 and 3) showing that eddy covariance method tends to underestimate the fluxes when eddy covariance device is placed higher above the water surface. Hence, use of the bulk gradients across a distance of ~1 m or greater may lead to unrealistic estimates of turbulent fluxes. Comparison of MEP-modeled fluxes with observations thus suffers from the limitation of large uncertainties sometimes comparable to the magnitudes of the actual fluxes. In addition, the bulk transfer equations are not energy constrained. The MEP-modeled E and H over water surfaces do not use wind speed, humidity, and temperature gradient data. Hence, they are not affected by the measurement errors of these variables. Since the MEP model is based on the conservation of energy, the MEP model-predicted fluxes are always consistent with radiation forcing; i.e., their magnitudes are bounded by R_n. This is clearly demonstrated by E and R_n during days 22–24 shown in Figures 1a and 2b, respectively, as discussed above.

There is more evidence in support of the MEP model in the literature. An earlier study [*Bill et al.*, 1980] provided an observational confirmation of the MEP model-predicted Bowen ratio in equation (10). *Bill et al.* [1980, Figure 5] showed a Bowen ratio of ~0.7 at lake surface temperature 14°C [*Bill et al.*, 1980, Figure 3] using eddy covariance data, which is in close agreement with the MEP model-predicted Bowen ratio as shown in Figure 2 of *Wang and Bras* [2011].

When the conductive cool skin is disturbed under strong wind conditions (e.g., >~15 m s^{-1}), the thermal inertia parameter is dependent on the eddy diffusivity, which may be formulated using a formal similarity between the oceanic and atmospheric boundary layer structures [*Gargett*, 1989] as the Monin-Obukhov similarity theory was applied to modeling turbulent diffusion in both the atmospheric boundary layer and the ocean mixed layer [*Large et al.*, 1994; *Kantha and Calyson*, 1994]. The MEP model-predicted heat fluxes are not sensitive to the parameterization of eddy diffusivity due to the square root dependence of thermal inertia on the diffusivity parameter.

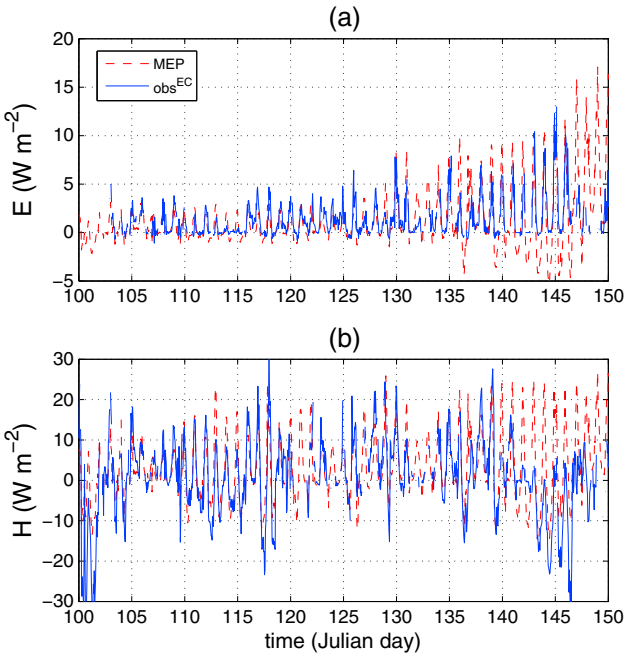

Figure 6. MEP model-predicted (a) latent heat flux E and (b) sensible heat flux H, according to equations (9) and (10) using measured R_n and T_s, versus eddy covariance measurements of E and H from SHEBA experiment at a ice pack of the Arctic Ocean during 10 April to 30 May 1998.

4.1.2. Snow Surface

Data set from FLUXNET, a worldwide network of energy, water and carbon flux observations, collected at a grassland site in Lethbridge Grassland, Alberta, Canada (AB-GRL), provided eddy covariance (EC) measurements of latent and sensible heat fluxes over snow-covered surface over the period of 1998–2008. Detailed description of the experiment site can be found in *Flanagan and Johnson* [2005]. Other surface meteorological variables including net radiation and air temperature at 1 m (as a surrogate for snow skin temperature that was not measured at the site) at 30 min resolution are used in this study. Figure 5 compares the MEP model-predicted E and H with the observed E and H during 1–10 December 2007. Using only the data of net radiation and surface temperature, the MEP model is able to capture the diurnal cycle of E and H and the modeled fluxes are in close agreement with the observations. The noisy EC H data appear to be caused by sampling error as the measured net radiation (not shown) following a well-defined diurnal cycle without rapid fluctuations.

4.1.3. Ice Surface

The Surface Heat Budget of the Arctic Ocean (SHEBA) experiment [*Uttal et al.*, 2002] provided field observations of turbulent fluxes over sea ice over the Arctic Ocean. The data collected during the Phase II of SHEBA (1997–1999), a year-long field campaign (2 October 1997 to 12 October 1998), are used in this study. The measurements of turbulent fluxes using eddy covariance and bulk aerodynamic method together with other surface meteorological variables including four components of radiation were archived at hourly resolution. More details about the field experiment and the data products are described in *Uttal et al.* [2002].

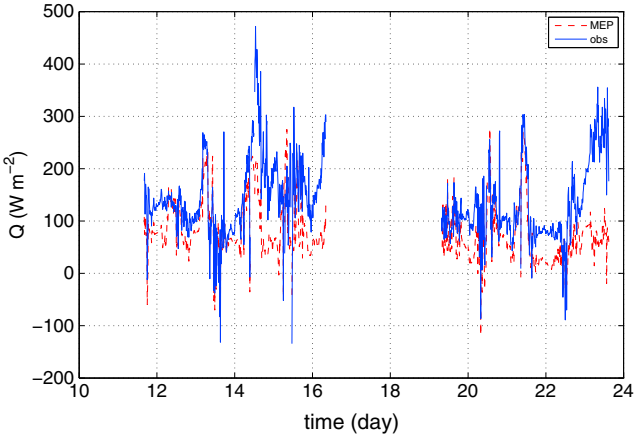

Figure 7. MEP model-predicted Q , according to equation (11) with observed R_s^n (as an input), and the MEP-modeled H (shown in Figure 1b), versus observational Q computed from the energy balance equation (4), $Q = R_l^n - E - H$, where the measured E, H, and R_l^n over Lake Råksjö from NOPEX experiment during 10–24 June 1994.

Figure 6 compares the MEP model-predicted E and H with the SHEBA eddy covariance fluxes over the period of 10 April to 30 May 1998 before melting of the sea ice as indicated by T_s record (data not shown). The magnitudes and diurnal cycles of the observed E (solid blue of Figure 6a) and H (solid blue of Figure 6b) are well captured by the MEP model (broken red). The visible differences between the MEP model-predicted and observed fluxes existed for about 5 days before the melting of ice sheet starting 28 May (day 148). It is unclear whether the relatively large nighttime $E < 0$ (deposition of water vapor) and daytime $H > 0$ predicted by the MEP model during days 141–147 are realistic

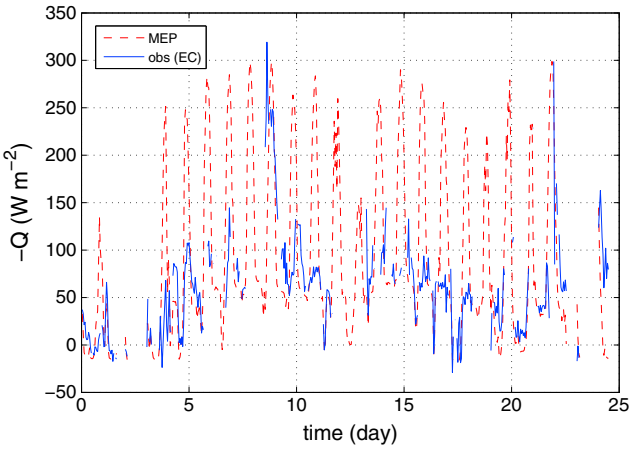

Figure 8. MEP model-predicted Q , according to equation (11) with observed R_s^n (as an input), and the MEP-modeled H (shown in Figure 3b), versus observational Q computed from the energy balance equation (4), $Q = R_l^n - E - H$, where the measured E, H, and R_l^n from the CALNEX cruise during 14 May to 7 June 2010.

because of missing air temperature and humidity data (at 2.5 m level), which are more indicative of upward versus downward transport of heat and water vapor. Since large positive (negative) daytime (nighttime) E and H are expected to concur due to the fact that the transport of heat and water vapor is caused by the same turbulent mixing process, the MEP- modeled fluxes are consistent with the observations.

4.2. Test of the MEP Model of Q

4.2.1. Water Surface

Figure 7 compares the MEP model-predicted and observed Q for Lake Råksjö. The MEP-modeled Q in equation (11) is derived using the observed $R_l^n (= R_n - R_s^n)$ (where R_n and R_s^n were directly measured during the field experiment) and the MEP model-predicted H and E equations (9) and (10) (Figure 1b) using R_n and T_s data. The MEP-modeled and observed Q are in reasonable agreement at least qualitatively. The noisy observed Q is caused by the noisy data of E and H (Figure 1). The largest differences between modeled and observed Q occurred during day 23 when measured E reached 300 W m^{-2} while the modeled E was below 100 W m^{-2}. The measurement error of E was more than +100 W m^{-2} when the observed R_n was below 200 W m^{-2} (Figure 2). Apparent observation errors of Q also occurred during day 14 when observed $-Q$ was substantially greater than that during the day before and after while R_n for day 14 was nearly identical to that for the day before and after. It was evident that wind speed during day 14 was stronger than wind speed during the day before and after. Note that day 23 had strongest wind during the 2 week period. It appears that the errors of E and H data (using the bulk transfer method) are responsible for the discrepancy between the modeled and observed fluxes as bulk transfer method tends to overestimate the fluxes under the condition of strong wind due to linear dependence of the empirical transfer coefficient on wind speed. The agreement between the modeled and observed Q is closer than those between the modeled and observed E and H (Figure 1) since Q is related to the total turbulent fluxes. Positive $-Q$ by definition implies transport of thermal energy from the water into the atmosphere, as expected, since the solar radiation absorbed within the water layer is the energy source of the surface heat fluxes. This case study confirms the possibility of modeling Q without using measurements below the water surfaces such as mixed layer water temperature in the bulk transfer equations and avoiding large uncertainty in the wind speed-dependent transfer coefficients in the bulk transfer equations.

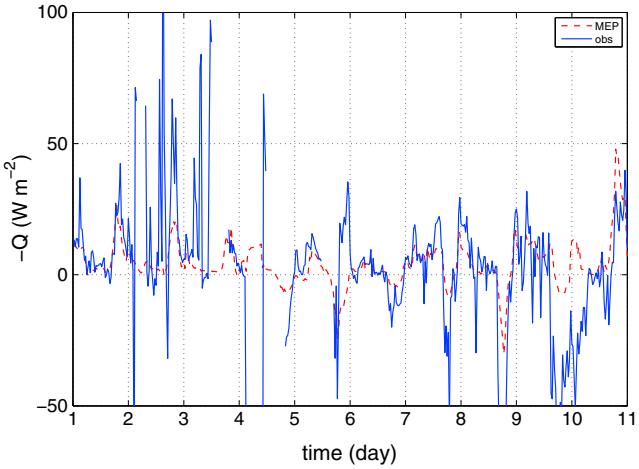

Figure 9. MEP model-predicted Q, according to equation (11) with observed R_l^n (as an input) and the MEP-modeled H (shown in Figure 1b), versus observational Q computed from the energy balance equation (4), $Q = R_l^n - E - H$, calculated from the measured E, H, R_n, and R_s^n at FLUXNET AB-GRL site during 1–10 December 2007.

Figure 8 compares the MEP model-predicted and observed Q for the CALNEX2010 cruise period. Agreement between the modeled and observed Q during 23 May and 3–7 June is evident, consistent with the test of modeled versus observed E and H. Underestimates of daytime E and

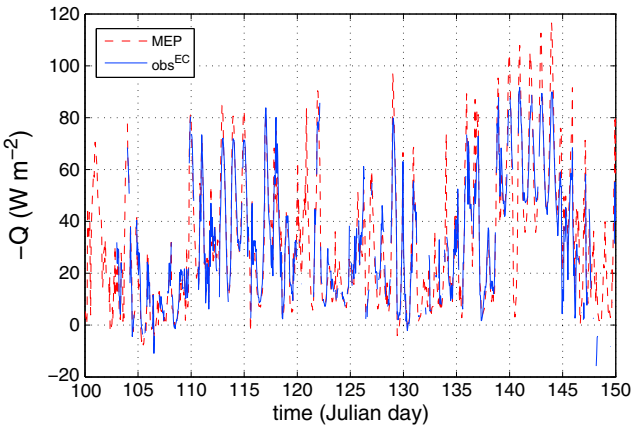

Figure 10. MEP model-predicted Q, according to equation (11) using measured R_s^n with the MEP-modeled H (Figure 1b), versus observational Q computed from the energy balance equation (4), $Q = R_l^n - E - H$, using the measured E, H, and R_l^n) from SHEBA experiment during 10 April to 30 May 1998.

H by eddy covariance method lead to underestimates of daytime Q, while the modeled and observed Q agree well during nighttimes. Positive $-Q$ again suggests transfer of thermal energy from the ocean to the atmosphere as for the case of Lake Råksjö as expected.

4.2.2. Snow Surface

Figure 9 compares the MEP model-predicted Q at the FLUXNET AB-GRL site during 1 to 10 December 2007. The MEP model-predicted Q is in good agreement with the observed Q despite the noisy data Q caused by unrealistic fluctuations in the eddy covariance data of H (Figure 5b). The spurious large values of H are inconsistent with the observed R_n (not shown). Negative Q again indicates that the loss of thermal energy balances the turbulent fluxes and long-wave radiation loss over the snow surface. The magnitude and diurnal cycle of the MEP model-predicted Q is consistent with previous studies [e.g., *Tarboton and Luce*, 1996; *Jeffries and Morris*, 2006].

4.2.3. Ice Surface

Figure 10 compares the MEP model-predicted Q with the observed Q from SHEBA data set over the period of 10 April to 30 May 1998. The observed diurnal cycles and magnitudes of Q are well captured by the MEP model. Negative Q implies that the loss of thermal energy of the ice sheet, like water and snow layer (see Figure 7), is the energy source of the turbulent heat fluxes and net long-wave radiation over the sea ice surface.

4.2.4. Test of the Consistency of the MEP and Physically Based Model of Q

The hourly Woods Hole Oceanographic Institution (WHOI) Improved Meteorology (IMET) BUOY data set (http://www.eol.ucar.edu/rdp/tcwids/tcwids.html) of the Tropical Ocean–Global Atmosphere (TOGA)-Coupled Ocean-Atmosphere Response Experiment(COARE) [*Webster and Lukas*, 1992] was used to test the consistency of the MEP and physically based model of Q. The extinction coefficients F_i and the characteristic penetration depth ζ_i in equation (16) for sea water are taken from *Defant* [1961] given in Table 2 [*Paulson and Simpson*, 1981]. Figure 11 shows the Q predicted by the two models using the input of R_s^n, R_l^n, and T_s from the TOGA-COARE WHOI IMET BUOY data for November 1992. The close agreement between the two models is evident. Given that the MEP model of Q is derived without solving heat transfer equation (e.g., equation (13)), the consistency of the two models is a strong justification of the MEP model. The consistency also justifies the MEP model of E and H since Q, E, and H are solved simultaneously from equations (9) to (11).

Table 2. The Extinction Coefficients F_i and the Characteristic Penetration Depths ζ_i in Equation (16) for Seawater [*Defant*, 1961] Cited by *Paulson and Simpson* [1981]

i	F_i	ζ_i (m)
1	0.237	34.8
2	0.360	2.27
3	0.179	3.15×10^{-2}
4	0.087	5.48×10^{-3}
5	0.080	8.32×10^{-4}
6	0.0246	1.26×10^{-4}
7	0.025	3.13×10^{-4}
8	0.007	7.82×10^{-5}
9	0.0004	1.44×10^{-5}

4.3. On the MEP Model and Its Application

The formulation of the MEP is built on the well-known physics including Fourier's law for heat conduction, Monin-Obukhov similarity theory for atmospheric boundary layer turbulence, and Clausius-Clapeyron equation for saturation vapor pressure. The MEP method, used as an inference algorithm instead of a physical principle, extracts the most relevant information about the surface fluxes provided by the radiant fluxes and surface temperature in the sense that the MEP model-predicted fluxes are the most probable partition of a radiant energy under the condition of given temperature. Wind speed and temperature and moisture gradient independent expressions of the fluxes should not be interpreted as that the fluxes are physically independent of these

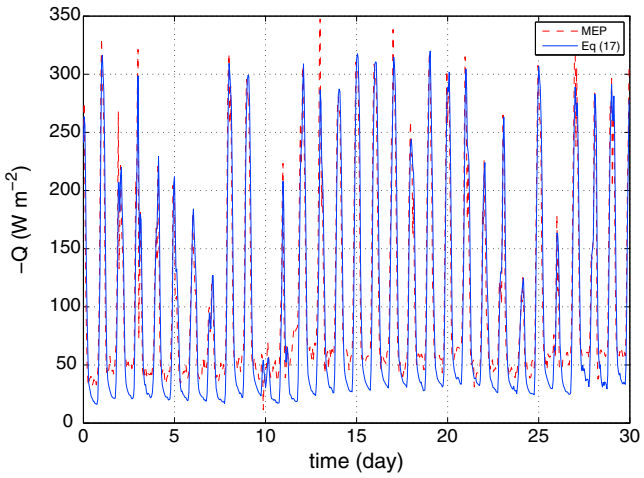

Figure 11. The MEP model-predicted Q (broken red) according to equation (11) versus the physical model of Q according to equation (17) (solid blue) using the input of T_s and R_s^n from TOGA-COARE WHOI IMET BUOY data during November 1992.

variables. In fact, the effect of wind speed or wind shear and temperature/moisture gradient on the fluxes has been represented in the model through the parameterization of boundary-layer turbulence using the Monin-Obukhov similarity equations. The MEP formulation removes the redundant information in the surface temperature/moisture and the near-surface temperature/moisture related to the fluxes. Effectiveness in utilizing information makes the MEP model parsimonious in input data and model parameters.

In addition to parsimony of input data and model parameters, the MEP model has a unique advantage of being radiant energy constrained and thus producing automatically a balanced surface energy budget. Fluxes expressed as analytical functions of net surface radiation provide an efficient approach of relating the uncertainties of the modeled heat fluxes to those of the radiative fluxes data. Accuracy of surface radiative fluxes estimates has more control on the reliability of the MEP-modeled surface heat fluxes over oceans than the modeled fluxes over land surfaces since variability in sea surface temperature and humidity are limited. Consequently, the ever-improving data products of surface radiative fluxes will lead to better estimates of the surface heat fluxes using the MEP model. It remains challenging to close the global surface energy budget despite progresses made in the past several years to reduce the uncertainties in global surface radiative fluxes estimates, especially the downwelling long-wave radiative fluxes [*Stephens et al.*, 2012], for producing surface irradiance estimates consistent with the top-of-atmosphere irradiances [*Kato et al.*, 2013]. Implementation of the MEP model in surface heat flux estimates will further reduce the error bounds of the heat fluxes. Compared to bulk transfer formula, MEP-based fluxes estimates eliminate the extra uncertainties associated with observation/simulation errors in surface wind speed and temperature/moisture gradients and brings us closer to the goal of producing a closed global surface energy budget. This makes MEP model an appealing tool for the studies aiming at detecting long-term trends and variabilities in various surface energy budget terms.

5. Conclusions

The MEP model of heat fluxes developed for land surfaces has been generalized to water-snow-ice surfaces. The reported case studies indicate that the MEP model is able to predict simultaneously the energy fluxes without using temperature and moisture gradient, wind speed, and surface roughness data. The MEP model-predicted surface fluxes are radiant energy constrained and satisfy automatically the surface energy balance. The parsimony of input data and model parameters make the MEP model not only an attractive surface fluxes retrieval algorithm for field experiments and remote sensing missions but also an advantageous physical parameterization of surface energy budget for regional and global climate models. The encouraging tests of the model has motivated an ongoing research to use the MEP model for remote sensing of the heat fluxes over water-snow-ice surfaces at global scales as field observations remain sparse and sporadic over water-snow-ice-covered regions. Another ongoing research is to incorporate the MEP model, as an alternative parameterization of surface energy budget, into regional and global coupled ocean-atmospheric models for the study of air-sea fluxes-driven processes such as the Madden-Julian oscillation.

Appendix A: Derivation of Equation (17)

Defining a new variable $\Theta = T - T_0$ that satisfies the following governing equation and initial/boundary condition according to equation (13)–(15):

$$\frac{\partial \Theta}{\partial t} = \kappa \frac{\partial^2 \Theta}{\partial z^2} + \frac{\partial}{\partial z}\left[\frac{R_s^n(t)}{\rho c} I(z)\right] \tag{A1}$$

$$\Theta = 0, \quad \text{for} \quad t = 0, \quad z < 0, \tag{A2}$$

$$\Theta = 0, \quad \text{for} \quad t > 0, \quad z \to -\infty, \tag{A3}$$

where R_s^n is the net short-wave radiation at the water-snow-ice surface defined in equation (2).

Laplace transform of equation (A1) with respect to t with the use of equation (A2) leads to

$$s\tilde{\Theta}(z,s) = \kappa \frac{\partial^2 \tilde{\Theta}}{\partial z^2} + \frac{\tilde{R}_s^n}{\rho c} \frac{\mathrm{d}I(z)}{\mathrm{d}z} \tag{A4}$$

where the Laplace transform, $\mathcal{L}$, is defined as

$$\mathcal{L}\{\Theta\} \equiv \tilde{\Theta}(z,s) = \int_0^\infty \mathrm{e}^{-st}\Theta(z,t)\mathrm{d}t \tag{A5}$$

$$\mathcal{L}\{Q_s\} \equiv \tilde{Q}_s(s) = \int_0^\infty \mathrm{e}^{-st}Q_s(t)\mathrm{d}t. \tag{A6}$$

The general solution of equation (A4) under the condition of equation (A3) is

$$\tilde{\Theta}(z,s) = A\exp\left(z\sqrt{\frac{s}{\kappa}}\right) + \frac{\tilde{R}_s^n(s)}{\rho c}\sum_i \left(s - \frac{\kappa}{\zeta_i^2}\right)^{-1} \frac{F_i}{\zeta_i}\exp\left(\frac{z}{\zeta_i}\right) \tag{A7}$$

where A is an arbitrary function of s and $I(z)$ is given in equation (16). Differentiation of both sides of equation (A7) with respect to z results in

$$\frac{\partial}{\partial z}\tilde{\Theta}(z,s) = \sqrt{\frac{s}{\kappa}}\tilde{\Theta}(z,s) - \frac{\tilde{R}_s^n(s)}{\rho c\sqrt{\kappa}}\sum_i \left(\sqrt{s} + \frac{\sqrt{\kappa}}{\zeta_i}\right)^{-1} \frac{F_i}{\zeta_i}\exp\left(\frac{z}{\zeta_i}\right). \tag{A8}$$

The first term on the left-hand side of equation (A8) is the Laplace transform of a half-order derivative with respect to t of $\Theta(z,t)$ [e.g., *Miller and Ross*, 1993]. Half-order derivative of a function is defined in *Miller and Ross* [1993]. Equation (A8) also implies

$$\tilde{Q}(z,s) = \rho c\sqrt{\kappa}\sqrt{s}\tilde{\Theta}(z,s) - \sum_i \left(\sqrt{s} + \frac{\sqrt{\kappa}}{\zeta_i}\right)^{-1} \frac{\sqrt{\kappa}}{\zeta_i}F_i\exp\left(\frac{z}{\zeta_i}\right)\tilde{R}_s^n(s), \tag{A9}$$

which can be used to derive expressions of Q in terms of T_s and R_s^n and T_s in terms of Q and R_s^n through inverse Laplace transforms.

Performing inverse Laplace transform, $\mathcal{L}^{-1}$, on equation (A8), we have

$$\begin{aligned}\frac{\partial}{\partial z}\Theta(z,t) = {} & \frac{1}{\sqrt{\kappa}}\frac{\partial^{\frac{1}{2}}}{\partial t^{\frac{1}{2}}}\Theta(z,t) - \frac{1}{\rho c\sqrt{\kappa}}\sum_i \frac{F_i}{\zeta_i}\exp\left(\frac{z}{\zeta_i}\right)\frac{1}{\sqrt{\pi}}\int_0^t \frac{R_s^n(s)\mathrm{d}s}{\sqrt{t-s}} \\ & + \frac{1}{\rho c}\sum_i \frac{F_i}{\zeta_i^2}\exp\left(\frac{z}{\zeta_i}\right)\int_0^t \exp\left[\frac{\kappa}{\zeta_i^2}(t-s)\right]\mathrm{erfc}\left(\frac{\sqrt{\kappa}}{\zeta_i}\sqrt{t-s}\right)R_s^n(s)\mathrm{d}s\end{aligned} \tag{A10}$$

where erfc is the complementary error function and the following equation is used

$$\mathcal{L}^{-1}\left\{\frac{1}{\sqrt{s}+\lambda}\right\} = \frac{1}{\sqrt{\pi t}} - \lambda\exp(\lambda^2 t)\mathrm{erfc}(\lambda\sqrt{t}) \tag{A11}$$

where λ is a constant.

As a result of equation (A10), $Q(z,t)$ can be written in terms of the time history of temperature and solar radiative flux as

$$\begin{aligned}Q(z,t) = \rho c\kappa\frac{\partial}{\partial z}T(z,t) = {} & \rho c\sqrt{\kappa}\frac{1}{\sqrt{\pi}}\int_0^t \frac{\partial T(z,s)}{\partial s}\frac{\mathrm{d}s}{\sqrt{t-s}} - \sum_i \frac{\sqrt{\kappa}}{\zeta_i}F_i\exp\left(\frac{z}{\zeta_i}\right)\frac{1}{\sqrt{\pi}}\int_0^t \frac{R_s^n(s)\mathrm{d}s}{\sqrt{t-s}} \\ & + \int_0^t \sum_i \frac{\kappa}{\zeta_i^2}F_i\exp\left(\frac{z}{\zeta_i}\right)\exp\left[\frac{\kappa}{\zeta_i^2}(t-s)\right]\mathrm{erfc}\left(\frac{\sqrt{\kappa}}{\zeta_i}\sqrt{t-s}\right)R_s^n(s)\mathrm{d}s\end{aligned} \tag{A12}$$

where s is the integration variable. Applying equation (A10) at the surface $z \to 0$ leads to the desired solution of Q.

Appendix B: Algorithm for Numerical Integration of Equation (17)

The first two terms in equation (17) require calculating a singular integral in the form,

$$\int_0^t \frac{g(s)\mathrm{d}s}{\sqrt{t-s}}.$$

Assume that the total integration domain $[0, t]$ is divided into n intervals $[t_i, t_{i+1}]$ for $i = 1, ..., n$. Over the ith interval $[t_i, t_{i+1}]$

$$\int_{t_i}^{t_{i+1}} \frac{g(s)\mathrm{d}s}{\sqrt{t-s}} \simeq \tilde{g}^i \int_{t_i}^{t_{i+1}} \frac{\mathrm{d}s}{\sqrt{t-s}} = -2\tilde{g}^i \int_{t_i}^{t_{i+1}} \mathrm{d}\sqrt{t-s} = 2\tilde{g}^i \left(\sqrt{t-t_i} - \sqrt{t-t_{i+1}}\right)$$

where $\tilde{g}^i$ represents the discretization of integrand g over $[t_i, t_{i+1}]$. The following approximation of g may be used:

$$\tilde{g}^i = \frac{g(t_{i+1}) - g(t_i)}{t_{i+1} - t_i},$$

when g is a derivative function, e.g., $g = \mathrm{d}T_s/\mathrm{d}s$, or

$$\tilde{g}^i = \frac{1}{2}[g(t_{i+1}) + g(t_i)],$$

when g is an ordinary function.

The third term in equation (17) is a convolution integral with a weight function involving an exponential function and a complementary error function. For large independent variables, the exponential function becomes extremely large while the complementary error function very small. This behavior may cause overflow and/or underflow in computing. To avoid this difficulty in programming, the following approach is recommended.

Rewrite $\exp(a^2 t)\mathrm{erfc}(a\sqrt{t})$ as

$$\mathrm{e}^{a^2 t}\mathrm{erfc}(a\sqrt{t}) = \frac{1}{\sqrt{\pi}} \int_0^\infty \frac{\mathrm{e}^{-u}\mathrm{d}u}{\sqrt{u + a^2 t}}.$$

Over the ith interval $[t_i, t_{i+1}]$, Q_s may be approximated as $(Q_s(t_i) + Q_s(t_{i+1}))/2$. Then

$$\begin{aligned}
\int_{t_i}^{t_{i+1}} \exp\left[\frac{\kappa}{\zeta_i^2}(t-s)\right] \mathrm{erfc}\left(\frac{\sqrt{\kappa}}{\zeta_i}\sqrt{t-s}\right) Q_s(s)\mathrm{d}s &\simeq \frac{1}{2}[Q_s(t_i) + Q_s(t_{i+1})] \int_{t_i}^{t_{i+1}} \exp[a^2(t-s)]\mathrm{erfc}(a\sqrt{t-s})\mathrm{d}s \\
&= \frac{1}{2}[Q_s(t_i) + Q_s(t_{i+1})] \frac{1}{\sqrt{\pi}} \int_{t_i}^{t_{i+1}} \left(\int_0^\infty \frac{\mathrm{e}^{-u}\mathrm{d}u}{\sqrt{u + a^2(t-s)}}\right)\mathrm{d}s \\
&= \frac{1}{2}[Q_s(t_i) + Q_s(t_{i+1})] \frac{1}{\sqrt{\pi}} \int_0^\infty \mathrm{e}^{-u}\mathrm{d}u \int_{t_i}^{t_{i+1}} \frac{\mathrm{d}s}{\sqrt{u + a^2(t-s)}} \\
&= \frac{1}{2}[Q_s(t_i) + Q_s(t_{i+1})] \frac{2}{a^2\sqrt{\pi}} \int_0^\infty \mathrm{e}^{-u} \left[\sqrt{u + a^2(t-t_i)}\right. \\
&\quad \left. - \sqrt{u + a^2(t-t_{i+1})}\right]\mathrm{d}u
\end{aligned} \tag{B1}$$

where $a^2 = \kappa/\zeta_i^2$. The integral in equation (B1) can be accurately calculated using the Laguerre integration formula:

$$\int_0^\infty \mathrm{e}^{-x} f(x) = \sum_{i=1}^n w_i f(x_i)$$

where x_i are the zeros of Laguerre polynomials of order n and w_i the corresponding weight factors. Laguerre polynomials of order 15 give satisfactory results.

Acknowledgments
This work was supported by NSF grants EAR-0943356 and EAR-1138611 and ARO grants W911NF-10-1-0236/W911NF-12-1-0095. We thank Judith A. Curry of Georgia Institute of Technology and Carol Anne Clayson of Florida State University for their generosity in preparing the SEAFLUX data product, Sven Halldin of Uppsala University to provide the NOPEX data product, and Chris W. Fairall of NOAA ESRL to offer the CALNEX 2010 cruise air-sea fluxes data used in this study. We thank Charmaine Hrynkiw of Meteorological Service of Canada, Betsy Sheffield of NSIDC User Service at University of Colorado, and Mary J. Saddington of NASA Langley ASDC User Service for making the FLUXNET data available. We are grateful to Soroosh Sorooshian and Dan Braithwaite for providing computer support at University of California at Irvine where part of the work reported in this paper was conducted. The comments of two anonymous reviewers greatly improved the quality of this paper.

References

Andreas, E. L., and B. Murphy (1986), Bulk transfer coefficients for heat and momentum over leads and polynyas, *J. Phys. Oceanogr.*, *16*, 1875–1883.
Best, M. J., et al. (2011), The Joint UK Land Environment Simulator (JULES), model description. Part 1: Energy and water fluxes, *Geosci. Model Dev.*, *4*, 677–699.
Bill, R. G., A. F. Cook, L. H. Allen, J. F. Bartholic, and T. Maki (1980), Predicting fluxes of latent and sensible heat of lakes from surface water temperature, *J. Geophys. Res.*, *85*(C1), 507–512.
Blyth, E., J. Gash, A. Lloyd, M. Pryor, G. P. Weedon, and J. Shuttleworth (2010), Evaluating the JULES land surface model energy fluxes using FLUXNET data, *J. Hydrometeorol.*, *11*, 509–519.
Boyle, J. P. (2007), Field results from a second-generation ocean/lake contact heat flux, solar irradiance, and temperature measurement instruments—The multisensor float, *J. Atmos. Oceanic Technol.*, *24*, 856–976.
Caisley, B., H. Lister, and L. Molyneux (1963), Measurement of profiles of wind speed, temperature and vapour pressure near to the ground, *General Assembly of Berkeley*, IASH Publication no. 61, 37–48.
Chou, S.-H., E. Nelkin, J. Ardizzone, R. M. Atlas, and C.-L. Shie (2003), Surface turbulent heat and momentum fluxes over global oceans based on the Goddard satellite retrieval, version 2 (GSSTF2), *J. Clim.*, *16*, 3256–3273.
Colbeck, S. C. (1989), Snow-crystal growth with varying surface temperature and radiation penetration, *J. Glaciol.*, *36*(119), 23–29.
Curry, J. A., C. A. Clayson, W. B. Rossow, R. Reeder, C. Y-Zhang, P. J. Webster, G. Liu, and R.-S. Sheu (1999), High-resolution satellite-derived dataset of the surface fluxes of heat, freshwater, and momentum for the TOGA COARE IOP, *Bull. Am. Meteorol. Soc.*, *80*, 2059–2080.
Dai, Y., et al. (2003), The common land model, *Bull. Am. Meteorol. Soc.*, *84*(8), 1013–1023.
Dewar, R. C. (2005), Maximum entropy production and the fluctuation theorem, *J. Phys. A: Math. Gen.*, *38*, L371–L381.
Dewar, R. C., and A. Maritan (2013), A theoretical basis for maximum entropy production, in *Beyond the Second Law: Entropy Production and Non-Equilibrium Systems*, edited by R. Dewar, pp. 49–71, Springer, Berlin Heidelberg.
Defant, A. (1961), *Physical Oceanography*, vol. 1, 729 pp., Pergamon, New York.
Desborough, C. E., A. J. Pitman, and P. Irannejad (1996), Analysis of the relationship between bare soil evaporation and soil moisture simulated by 13 land surface schemes for a simple non-vegetated site, *Global Planet. Change*, *13*, 47–56.
Dickinson, R. E., A. Henderson-Sellers, P. J. Kennedy, and M. F. Wilson (1986), Biosphere Atmosphere Transfer Scheme (BATS) for the NCAR Community Climate Model, *NCAR Tech. Note, TN-275+STR, 69*, Natl. Cent. for Atmos. Res., Boulder, Colo.
Fairall, C. W., E. F. Bradley, D. P. Rogers, J. B. Edson, and G. S. Young (1996a), Bulk parameterization of air-sea fluxes for Tropical Ocean Global Atmosphere Coupled Ocean-Atmosphere Response Experiment, *J. Geophys. Res.*, *101*(C2), 3747–3764.
Fairall, C. W., E. F. Bradley, J. S. Godfrey, G. A. Wick, J. B. Edson, and G. S. Young (1996b), Cool-skin and warm-layer effects on sea surface temperature, *J. Geophys. Res.*, *101*(C1), 1295–1308.
Flanagan, L. B., and B. G. Johnson (2005), Interacting effects of temperature, soil moisture and plant biomass production on ecosystem respiration in a northern temperate grassland, *Agric. For. Meteorol.*, *130*, 237–253.
Gargett, A. E. (1989), Ocean turbulence, *Annu. Rev. Fluid Mech.*, *21*, 419–451.
Granger, R. J., and N. Hedstrom (2011), Modelling hourly rates of evaporation from small lakes, *Hydrol. Earth Syst. Sci.*, *15*, 267–277.
Greuell, W., and J. Oerlemans (1989), The evolution of the Englacial temperature distribution in the superimposed ice zone of a polar ice cap during a summer season, in *Glacier Fluctuations and Climatic Change*, edited by J. Oerlemans, pp. 289–303, Kluwer Acad., Netherlands.
Halldin, S., S-E. Gryningb, L. Gottschalkc, A. Jochumd, L-C. Lundina, and A. A. Van de Griende (1999), Energy, water and carbon exchange in a boreal forest landscape—NOPEX experiences, *Agric. For. Meteorol.*, *98–99*, 5–29.
Hayashi, Y. (1981), Space-time cross spectral analysis using the maximum entropy method, *J. Meteorol. Soc. Jpn*, *59*(5), 620–623.
Henderson-Sellers, A., A. J. Pitman, P. K. Love, P. Irannejad, and T. H. Chen (1995), The project for intercomparison of land surface parameterization schemes(P ILPS): Phase 2 and 3, *Bull. Am. Meteorol. Soc.*, *76*(4), 489–503.
Henderson-Sellers, A., P. Irannejad, K. McGuffie, and A. Pitman (2003), Predicting land-surface climates—Better skills or moving targets?, *Geophys. Res. Lett.*, *30*(14), 1777, doi:10.1029/2003GL017387.
Heikinheimo, M., M. Kangas, T. Tourula, A. Venäläinen, and S. Tattari (1999), Momentum and heat fluxes over lakes Tämnaren and Råksjö determined by the bulk aerodynamic and eddy-correlation methods, *Agric. For. Meteorol.*, *98–99*, 521–534.
Jaynes, E. T. (1957), Information theory and statistics mechanics, *Phys. Rev.*, *106*, 620–630.
Jaynes, E. T., and G. L. Bretthorst (Ed.) (2003), *Probability Theory—The Logic of Science*, 755 pp., Cambridge Univ. Press, New York.
Jeffries, M. O., and K. Morris (2006), Instantaneous daytime conductive heat flow through snow on lake ice in Alaska, *Hydrol. Processes*, *20*, 803–815.
Kaiser, J. A. C., and K. G. Williams (1974), Measurement of the vertical heat flux in the upper ocean layer, *J. Phys. Oceanogr.*, *4*(2), 137–114.
Kantha, L. H., and C. A. Calyson (1994), An improved mixed layer model for geophysical applications, *J. Geophys. Res.*, *99*(C12), 25,235–25,266.
Kapur, J. N. (1989), *Maximum Entropy Models in Science and Engineering*, 635 pp., John Wiley, New York.
Kato, S., N. G. Loeb, F. G. Rose, D. R. Doelling, D. A. Rutan, T. E. Caldwell, L. Yu, and R. A. Weller (2013), Surface irradiances consistent with CERES-derived top-of-atmosphere shortwave and longwave irradiances, *J. Clim.*, *26*, 2719–2740.
Kiehl, J. K., and K. E. Trenberth (1997), Earth's annual global mean energy budget, *Bull. Am. Meteorol. Soc.*, *78*, 197–208.
Kleidon, A., and R. D. Lorenz (Ed.) (2005), *Non-equilibrium Thermodynamics and the Production of Entropy*, 260 pp.
Kleidon, A., and S. Schymanski (2008), Thermodynamics and optimality of the water budget on land, *Geophys. Res. Lett.*, *35*, L20404, doi:10.1029/2008GL035393.
Kleidon, A., Y. Malhi, and P. M. Cox (2010), Maximum entropy production in ecological environmental systems: Applications and implications, *Philos. Trans. R. Soc. London, Ser. B*, *365*, 1295–1455.
Kowalczyk, E. A., Y. P. Wang, and R. M. Law (2006), The CSIRO Atmospheric Biosphere Land Exchnage (CABLE) model for use in climate models and as an offline model, *CSIRO Marine and Atmospheric Research Paper 13*, CSIRO Marine and Atmospheric Research, Aspendale, Vic., Australia. [Available at http://www.cmar.csiro.au/e-print/open/kowalczykea_2006a.pdf.]
Khundzhua, G. G., A. M. Gusev, Y. G. Andreyev, V. V. Gurov, and N. A. Skorokhvatov (1977), Structure of the cold surface film of the ocean and heat transfer between the ocean and the atmosphere [English translation], *Atmos. Oceanic Phys.*, *13*, 506–509.
Large, W. G., J. C. McWilliams, and S. C. Doney (1994), Oceanic vertical mixing: A review and a model with a nonlocal boundary layer parameterization, *Rev. Geophys.*, *32*(4), 363–403.
Large, W. G., and S. G. Yeager (2009), The global climatology of an interannually varying air-sea flux data set, *Clim. Dyn.*, *33*, 341–364.
Lemone, M. A., M. Tewari, F. Chen, J. G. Alfieri, and D. Niyogi (2008), Evaluation of the Noah land surface model using data from a fair-weather IHOP_2002 day with heterogeneous surface fluxes, *Mon. Weather Rev.*, *136*, 4915–4941.

Liu, W. T., K. B. Katsaros, and J. A. Businger (1979), Bulk parameterization of air-sea exchanges of heat and water vapor including the molecular constraints at the interface, *J. Atmos. Sci.*, *36*, 1722–1735.
McJannet, D. L., F. J. Cook, R. P. McGloin, H. A. McGowan, and S. Burn (2011), Estimation of evaporation and sensible heat flux from open water using a large aperture scintillometer, *Water Resour. Res.*, *47*, W05545, doi:10.1029/2010WR010155.
Miller, K. S., and B. Ross (1993), *An Introduction to the Fractional Calculus and Fractional Differential Equations*, 366 pp., John Wiley, New York.
Mitchell, K. (2005), The community Noah land-surface model (LSM), *Users Guide Public Release Version 2.7.1*. [Available at ftp://ftp.emc.ncep.noaa.gov/mmb/gcp/ldas/noahlsm/ver_2.7.1.]
Moore, G. W. K., and I. A. Renfrew (2002), An assessment of the surface turbulent heat fluxes from the NCEP-NCAR reanalysis over the western boundary currents, *J. Clim.*, *15*, 2020–2037.
Mueller, B., et al. (2011), Evaluation of global observations based evapotranspiration datasets and IPCC AR4 simulations, *Geophys. Res. Lett.*, *38*, L06402, doi:10.1029/2010GL046230.
Oleson, K. W., et al. (2010), Technical description of version 4.0 of the Community Land Model (CLM), *NCAR Tech. Note, NCAR/TN-478+STR 266*, Natl. Cent. for Atmos. Res., Boulder, Colo.
Paltridge, G. W. (1975), Global dynamics and climate—A system of minimum entropy exchange, *Q. J. R. Meteorol. Soc.*, *101*, 475–484.
Paulson, C. A., and J. J. Simpson (1981), The temperature difference across the cool skin of the ocean, *J. Geophys. Res.*, *86*(C11), 11,044–11,054.
Ryerson, T. B., et al. (2013), The 2010 California Research at the Nexus of Air Quality and Climate Change (CalNex) field study, *J. Geophys. Res. Atmos.*, *118*, 5830–5866, doi:10.1002/jgrd.50331.
Saunders, P. (1967), Temperature at the ocean-air interface, *J. Atmos. Sci.*, *24*, 269–273.
Shipley, B. (2010), *From Plant Traits to Vegetation Structure: Chance and Selection in the Assembly of Ecological Communities*, 277 pp., Cambridge Univ. Press, New York.
Slatyer, R. O., and I. C. McIlroy (1961), *Practical Microclimatology*, 300 pp., Commonwealth Scientific and Industrial Research Organization Australia, UNESCO, Paris, France.
Soloviev, A. V., and P. Schlüssel (1996), Evolution of cool skin and direct air-sea gas transfer coefficient during daytime, *Boundary Layer Meteorol.*, *77*, 45–68.
Sromovsky, L. A., J. R. Anderson, F. A. Best, J. P. Boyle, C. A. GSisko, and V. E. Suomi (1999a), The Skin-layer Ocean Heat Flux Instrument (SOHFI). Part I: Design and laboratory characterization, *J. Atmos. Oceanic Technol.*, *14*, 1224–1238.
Sromovsky, L. A., J. R. Anderson, F. A. Best, J. P. Boyle, C. A. GSisko, and V. E. Suomi (1999b), The Skin-layer Ocean Heat Flux Instrument (SOHFI). Part II: Field measurements of surface heat flux and solar irradiance, *J. Atmos. Oceanic Technol.*, *14*, 1239–1253.
Stephens, G. L., M. Wild, P. W. Stackhouse, T. L'Ecuyer, S. Kato, and D. S. Henderson (2012), The global character of the flux of downward longwave radiation, *J. Clim.*, *25*, 2329–2340.
Suzuki, E. (1958), Weather Forecast and Entropy in Information Theory. *Meteorological Research Institute of Japan Meteorological Agency, Vol. IX*, No. 2, 52–62.
Tarboton, D. G., and C. H. Luce (1996), Utah energy balance snow accumulation and melt model (UEB), in *Computer Model Technical Description and Users Guide*, 66 pp., Utah Water Research Laboratory and USDA Forest Service Intermountain Research Station, Loganm UTah. [Available at http://www.engineering.usu.edu/dtarb/.]
Uttal, T., et al. (2002), Surface heat budget of the Arctic Ocean, *Bull. Am. Meteorol. Soc.*, *83*, 255–275.
Verkley, W. T. M., and P. Lynch (2009), Energy and enstrophy spectra of geostrophic turbulent flows derived from a maximum entropy principle, *J. Atmos. Sci.*, *66*(8), 2216–2236.
Wang, J., and R. L. Bras (1999), Ground heat flux estimated from surface soil temperature, *J. Hydrol.*, *216*, 214–226.
Wang, J., and R. L. Bras (2009), A model of surface heat fluxes based on the theory of maximum entropy production, *Water Resour. Res.*, *45*, W11422, doi:10.1029/2009WR007900.
Wang, J., and R. L. Bras (2010), An extremum solution of the Monin-Obukhov similarity equations, *J. Atmos. Sci.*, *67*(2), 485–499.
Wang, J., and R. L. Bras (2011), A model of evapotranspiration based on the theory of maximum entropy production, *Water Resour. Res.*, *47*, W03521, doi:10.1029/2010WR009392.
Wang, J., V. Nieves, and R. L. Bras (2013), MaxEnt and MaxEP in modeling fractal topography and atmospheric turbulence, in *Beyond the Second Law: Entropy Production and Non-Equilibrium Systems*, edited by R. Dewar et al., pp. 309–322, Springer, Berlin Heidelberg.
Wang, Y. P., E. Kowalczyk, R. Leuning, G. Abramowitz, M. R. Raupach, B. Pak, E. van Gorsel, and A. Luhar (2011), Diagnosing errors in a land surface model (CABLE) in the time and frequency domains, *J. Geophys. Res.*, *116*, G01034, doi:10.1029/2010JG001385.
Webster, P. J., and R. Lukas (1992), TOGA COARE: The Coupled Ocean-Atmosphere Response Experiment, *Bull. Am. Meteorol. Soc.*, *73*(9), 1377–1416.
Wolfe, D. E., and C. W. Fairall (2010), Ship-board flux measurements made during CalNex 2010, Abstract A21C-0100 presented at 2010 Fall Meeting, AGU, San Francisco, Calif., 13–17 Dec.
Yang, J., Z.-H. Wang, and T.-W. Lee (2013), Relative efficiency of surface energy partitioning over different land cover, *Br. J. Environ. Clim. Change*, *3*, 86–102.
Yang, Z.-L., and R. E. Dickinson (1996), Description of the Biosphere-Atmosphere Transfer Scheme (BATS) for the soil moisture workshop and evaluation of its performance, *Global Planet. Change*, *13*, 117–134.
Yen, Y.-C. (1981), Review of thermal properties of snow, ice and sea ice, *CRREL Report 81-10*, US Army Corps of Engineering, Cold Regions Research and Engineering Laboratory, Hanover, New Hampshire.
Zeng, X., M. Zhao, and R. E. Dickinson (1998), Intercomparison of bulk aerodynamic algorithms for the computation of sea surface fluxes using TOGA COARE and TAO data, *J. Clim.*, *11*, 2628–2644.